(Received 28 December 2023, Accepted 23 February 2024, Scheduled 5 March 2024)

An Energy Distribution Correlation Judgment Method for Interrupted Sampling Repeater Jamming Suppression

Ji Li, Fan Su, Wei Wang*, Rui Yan, and Jialiang Li

College of Computer and Communication Engineering, Changsha University of Science & Technology, Changsha 410000, China

ABSTRACT: Interrupted Sampling Repeater Jamming (ISRJ) can produce several false targets through intermittent sampling and forwarding of the intercepted signals. The paper proposes an interference identification and suppression method based on Short-Time Fourier Transform-Energy Distribution Correlation Judgment (STFT-EDCJ) to lessen the impact of the false targets mixed in echo pulses. Firstly, the method obtains the energy distribution of echoes in the time-frequency domain employing the short-time Fourier transform, extracts the time slice of higher energy targets through energy peak detection, and then calculates the Pearson correlation coefficient (PCC) of the energy distribution in the frequency domain of each target time slice to construct the Target PCC Datasets (TPCCD). Secondly, it distinguishes between the real target and false targets after echo pulse pressure by the range and specificity of TPCCD. Finally, it uses mapping the time domain position of the false targets to suppress interference. The abundant simulation results verify the proposed method's effectiveness, and the Monte Carlo simulation demonstrates the method's effectiveness under ISRJ models.

1. INTRODUCTION

With the improvement of Digital Radio Frequency Memory technology, active jammer has caused great trouble for the radar receiver to recognize the real target because of its adjustable mode and configurable parameters. Interrupted Sampling Repeater Jamming (ISRJ) is a spoofing pattern for Linear Frequency Modulation (LFM) pulse compression radar [1]. The jammer intermittently samples part of the pulse radar signal [2] and forwards the interference pulses coherent with the intercepted signal, and it can generate multiple false targets through the pulse compression characteristics [3–6]. Different jamming modes and interference parameters also have their own characteristics for the effect of false targets generated by jammers. Paper [7] analyzed the performance of different types of ISRJ and their interference characteristics.

In recent years, many scholars have studied the methods of interference suppression and interference recognition in various dimensions. According to the intermittent sampling characteristics of the ISRJ, [8] proposes a method based on the energy detection function to extract the signal segment with no ISRJ interference from the perspective of the energy domain. Paper [9] identifies the false targets based on the temporal energy distribution difference of the ISRJ and real target echo after pulse compression, and the evaluation is the variance of the energy distribution. Paper [10] constructs a matched filter to suppress interference based on the energy accumulation characteristics of ISRJ interference and target echoes after pulse compression. Paper [11] identifies real target echo through the correlation of high-resolution range profile. Paper [12] proposes that an adaptive filter can be constructed through the histogram energy analysis to suppress the ISRJ. Paper [13] uses a one-dimensional semi-parametric signal decomposition to estimate parameters of echo signals instead of time-frequency analysis and distinguishes interference and target by clustering method. Paper [14] obtains the time-frequency information of radar echo by STFT and has designed a detection model of target distance and velocity based on the convolution neural network (CNN) to counter the ISRJ. Paper [15] uses the fractional Fourier transform to identify the target echo in the echo signal after pulse compress and constructs a time-domain filter for interference suppression based on the sampled signal.

This paper focuses on the interference of multiple false targets caused by ISRJ interference on mixed echo pulse, and it obtains target information in the time domain, frequency domain, and energy domain through time-frequency analysis. The observation results of the target information have shown that the energy distribution of false targets generated by interference in the frequency domain has the characteristic of intermittent fluctuations, and the energy distribution of the real target generated by LFM pulse compression radar in the frequency domain shows a characteristic of being stable and continuous. Therefore, this paper proposes a cross-correlation judgment method to distinguish between the real target and false targets after echo pulse pressure based on the low cross-correlation between the frequency domain energy distributions of the two above.

The method first obtains the frequency energy distribution of targets through STFT on the target time series compressed by pulses. Secondly, the method extracts high-energy target time slices through energy peak detection and obtains the Pearson correlation coefficient (PCC) [16] data set corresponding to the frequency energy distribution of each target time slice by a cross-correlation algorithm. Once again, based on the low overall cross-correlation between the energy distribution of the real target and false targets after echo pulse pressure, the method splits Pearson coefficient data sets of each target to construct the

* Corresponding author: Wei Wang (wangwei@csust.edu.cn).

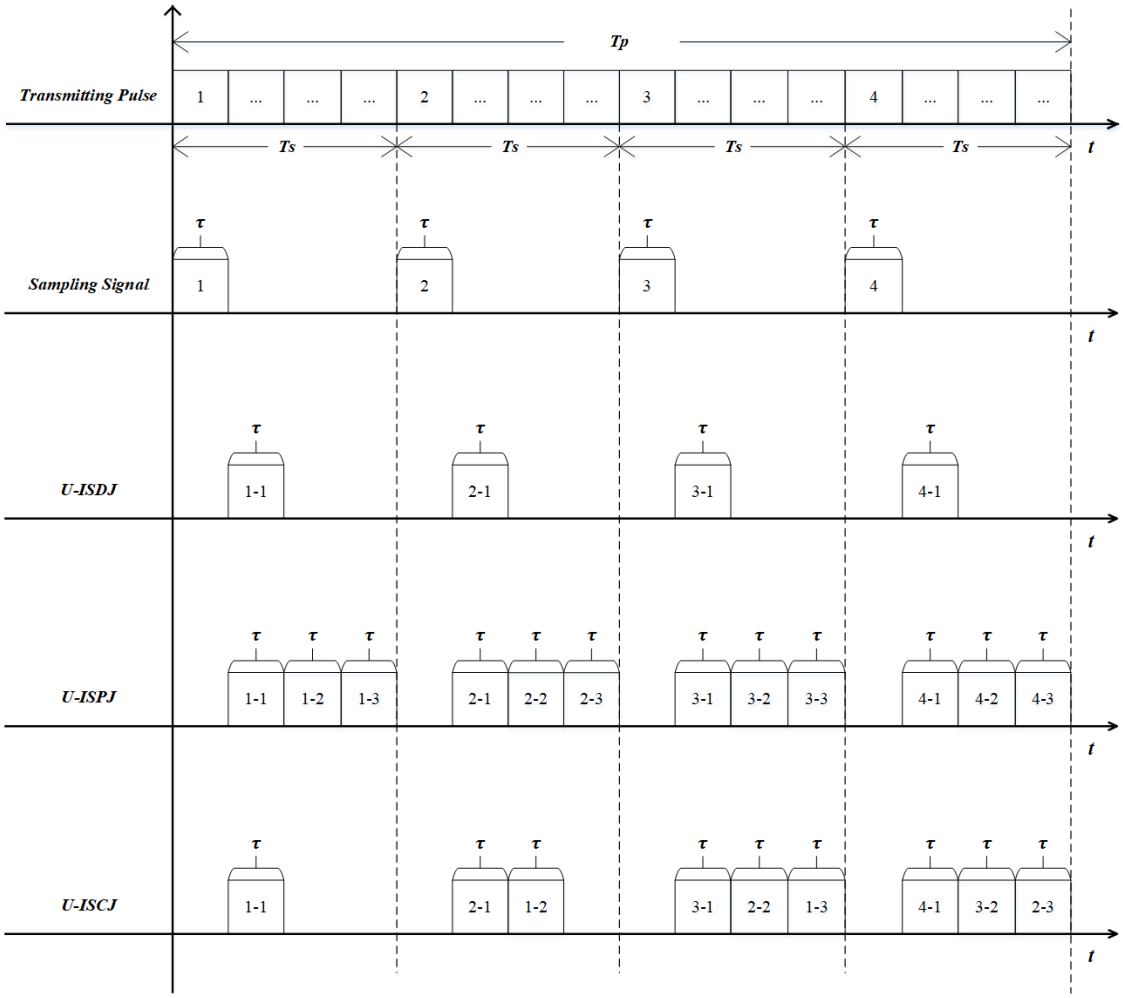

FIGURE 1. The working principle of U-ISDJ, U-ISPJ, and U-ISCJ.

target PCC datasets. Then, the method distinguishes between the real target and false targets based on the range and specificity of the target PCC datasets. Finally, this method takes the mapping target position as the center position and derives the position interval of the false targets in the time domain based on the short-time width of the short-time Fourier transform. At this point, it achieves interference suppression by setting the position interval to zero.

The remainder of the paper is structured as follows. The principle of various ISRJ interferences is introduced in Section 2. Section 3 introduces the method of correlation judgment and interference suppression. In Section 4, first various parameters from the applicability of the correlation judgment method are simulated, and then the interference suppression effect is analyzed under different signal-to-noise ratios, whereas the conclusion is given in Section 6. The comparative experimental simulation results of [15] using this method are presented in Section 5.

2. INTERFERENCE MODEL

The common three jamming methods include interrupted-sampling and direct repeater jamming (ISDJ) [1], interrupted-sampling and periodic repeater jamming (ISPJ) [17], and interrupted-sampling and cyclic repeater jamming (ISCJ) [18]. The jamming can be divided into uniform sampling and nonuniform sampling according to different sampling modes of jammer [19, 20].

2.1. Uniform-Interrupted Sampling Repeater Jamming

The principle of uniform-interrupted sampling is to take regular interval sampling on the intercepted signal, with the sampling pulse slice width and sampling period remaining unchanged for each sampling.

The working principle of U-ISDJ, U-ISPJ, and U-ISCJ is shown in Fig. 1.

According to Fig. 1, in the entire sampling process, the sampling signals by the three types of uniform intermittent sampling are the same, and the intermittent sampling period for each sampling is unchanged. The uniform intermittent sampling signal $X_{UIS}(t)$ is defined as:

$$X_{UIS}(t) = \sum_{n=1}^{N} rect\left(\frac{t-(n-1)T_s}{\tau_s}\right) S(t) \qquad (1)$$

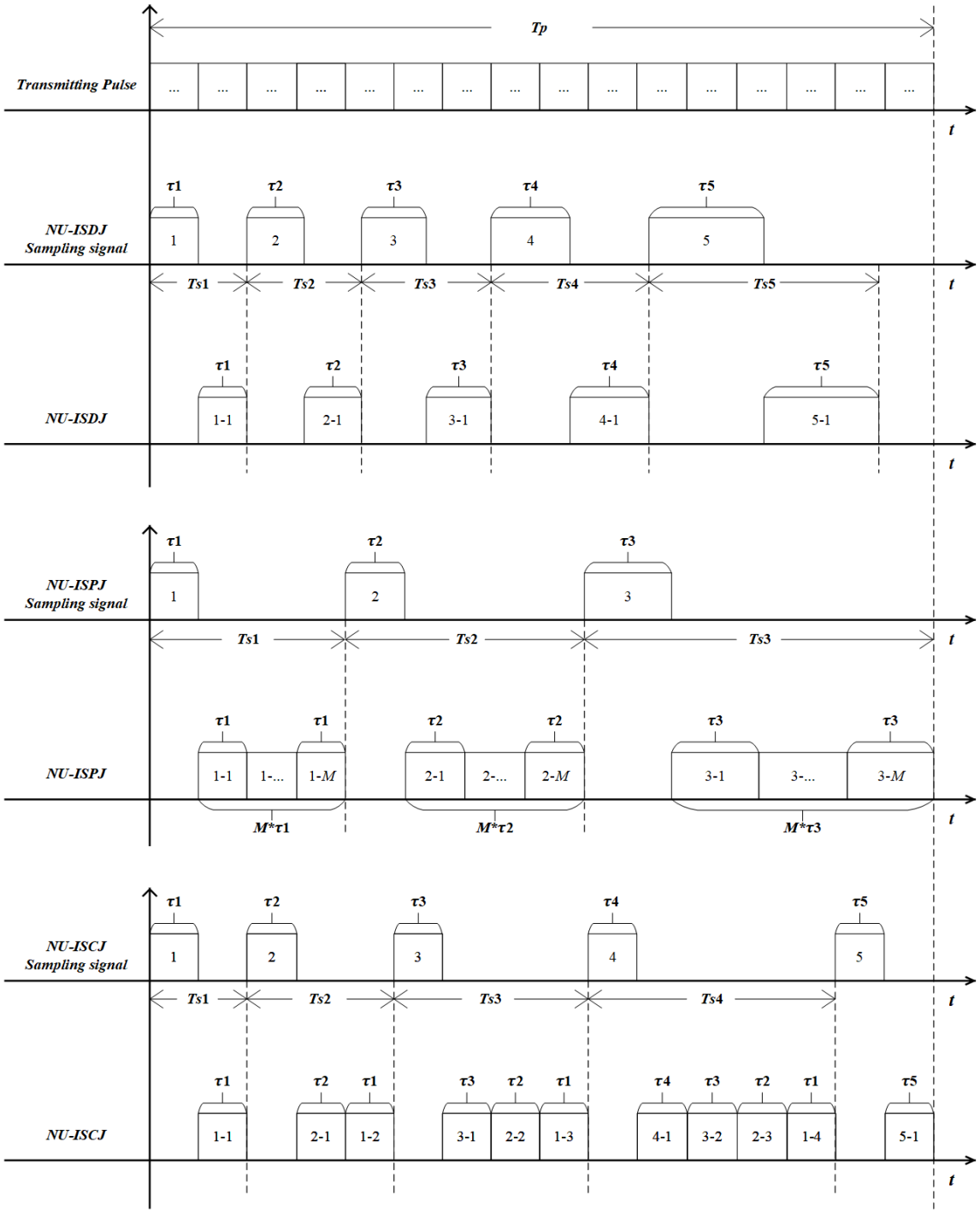

FIGURE 2. The working principle of NU-ISDJ, NU-ISPJ, and NU-ISCJ.

where $N = \lfloor T_p/T_s \rfloor$ represents the sampling times; T_p represents the width of the intercepted signal pulse; $T_s(n) = T_s$ represents the width of the sampling period corresponding to the nth sampling; $\tau_s = \tau$ is the width of sampling slices; the sampling time is equal to the forwarding time; $S(t)$ represents the intercepted signals.

U-ISDJ is equivalent to the delayed forwarding of the entire sampled signal $X_{UIS}(t)$, and the forwarding time is 1. The time domain expression of U-ISDJ is as follows:

$$X_{U\_ISDJ}(t) = \sum_{n=1}^{N} rect\left(\frac{t-(2n-1)\tau}{\tau}\right) S(t-\tau) \quad (2)$$

U-ISPJ is equivalent to the entire sampled signal $X_{UIS}(t)$ that performs delayed forwarding, and the number of forward times is related to the width of the sampling slice and sampling period.

Its time domain expression is:

$$X_{U\_ISPJ}(t) = \sum_{m=1}^{M}\sum_{n=1}^{N} rect\left(\frac{t - m\tau - (n-1)(M+1)\tau}{\tau}\right) S\left(t - m\tau\right) \tag{3}$$

where $M \leq \lfloor T_s/\tau \rfloor - 1$ is the forwarding times, and $m\tau$ is the delay corresponding to the mth forwarding.

The principle of U-ISCJ can be equivalent to forwarding the entire sampled signal $X_{UIS}(t)$ by increasing the delay successively. The time domain expression is:

$$X_{U\_ISCJ}(t) = \sum_{m=1}^{R}\sum_{n=0}^{N-1} rect\left(\frac{t - (m-1)T_s - (m+n)\tau}{\tau}\right) S\left(t - (m-1)T_s - m\tau\right) \tag{4}$$

where $(m-1)T_s + m\tau$ is the delay corresponding to the mth forwarding, and $R = \min\{N, M\}$ is the forwarding times of the entire sampled signal $X_{UIS}(t)$. $M \leq \lfloor T_s/\tau \rfloor - 1$ is the maximum value of forwarding times in a sampling period.

2.2. Nonuniform Interrupted Sampling Repeater Jamming

For nonuniform intermittent sampling, the sampling slice width for each sampling depends on the jammer's forwarding method and setting parameters.

The working principle of NU-ISDJ, NU-ISPJ, and NU-ISRJ is shown in Fig. 2.

According to Fig. 2, the sampling period for each sampling of NU-ISRJ is decided by the sampling slice width and forwarding mode. Each sampling begins at the location where the previous sampling period finishes.

Nonuniform intermittent sampling signal $X_{NUIS}(t)$ is defined as:

$$X_{NUIS}(t) = \sum_{n=1}^{N} rect\left(\frac{t - T_{s\_n}}{\tau_n}\right) S(t) \tag{5}$$

where N represents the maximum value of sampling times, $\tau_n = K * (n-1) * \tau_1$ represents the width of the sampling slice corresponding to the nth sampling; K represents the growth rate of sampling slice width for each sampling; and τ_1 represents the width of the sampling slice corresponding to the 1st sampling. T_{s_n} is the starting position of the nth sampling.

The expression of T_{s_n} is as follows:

$$T_{s\_n} = \begin{cases} 0, & n = 1 \\ \sum_{i=1}^{n-1} T_s(i), & 2 \leq n \leq N \end{cases} \tag{6}$$

NU-ISDJ forwards the sampling slice after each sampling, and each sample slice is only forwarded once. The total of the sampling slice width and forwarding slice width for this sampling determines the sampling period. The starting position of each forwarding depends on this sampling's sampling slice width and the previous sampling period.

The time domain expression of NU-ISDJ is as follows:

$$X_{NU\_ISDJ}(t) = \sum_{n=1}^{N} rect\left(\frac{t - T_{d\_n}}{\tau_n}\right) S(t) \tag{7}$$

where $T_{d\_n} = T_{s\_n}$ represents the starting position corresponding to the nth sampling, and $T_s(n) = 2\tau_n$ represents the width of the sampling period corresponding to the nth sampling. τ_n represents the width of the sampling slice corresponding to the nth sampling.

NU-ISPJ also forwards the sampling slice after each sampling, but each sampling slice is only forwarded more than once. NU-ISPJ is equivalent to the entire sampled signal $X_{NUIS}(t)$ that performs delayed forwarding. The time domain expression of NU-ISPJ is as follows:

$$X_{NU\_ISPJ}(t) = \sum_{m=1}^{M}\sum_{n=1}^{N} rect\left(\frac{t - m\tau_n - (n-1)T_{p\_n}}{\tau_n}\right) S\left(t - m\tau_n\right) \tag{8}$$

where $T_{p\_n} = T_{s\_n}$ represents the starting position corresponding to the nth sampling, and $T_s(n) = (M+1)\tau_n$ represents the width of the sampling period corresponding to the nth sampling. $M \geq 2$ is the forwarding times. $m\tau$ is the delay corresponding to the mth forwarding.

The principle of NUISCJ is that start from the first sampling period, combine the forwarding slices in this sampling period and the sampling slices in the next sampling period into a reverse order slice, and then forward the reverse order slices in the next sampling period [15], and repeat the above process until the entire sampling process is complete.

The time domain expression of NU-ISCJ is as follows:

$$X_{NU\_ISCJ}(t) = \sum_{m=1}^{N}\sum_{n=1}^{N-m+1} rect\left(\frac{t - \alpha(m)\tau_n - T_{c\_n}}{\tau_n}\right) S\left(t - T_{c\_n}\right) \tag{9}$$

where $T_{c\_n} = T_{s\_n}$ represents the starting position corresponding to the nth sampling, and $\alpha(m) = m(m+1)/2 + (m-1)$ represents the delay coefficient corresponding to the mth forwarding. τ_n represents the width of the sampling slices corresponding to the nth sampling.

There are two cases in which τ_n is selected, and its expression is as follows:

$$\begin{cases} \tau_n = \tau_1, & T_s(n) = (n+1) * \tau_1 \\ \tau_n = K * (n-1) * \tau_1, & T_s(n) = 2\tau_n + \sum_{i=1}^{n-1} \tau_n \end{cases} \tag{10}$$

where $T_s(n)$ represents the width of the sampling period corresponding to the nth sampling.

3. SHORT-TIME FOURIER TRANSFORM ENERGY DISTRIBUTION CORRELATION JUDGMENT

The interference identification and suppression method proposed in this paper is shown in Fig. 3. The method process

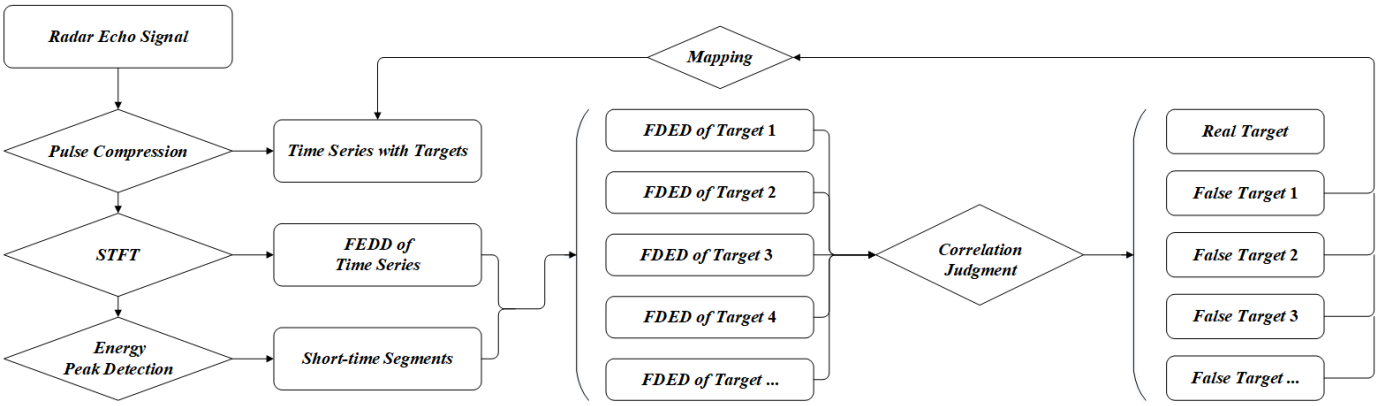

FIGURE 3. The schematic diagram of the method proposed in this article.

mainly includes Pulse Compression, Short-Time Fourier Transform, Energy Peak Detection, Correlation Judgment of Frequency Domain Energy Distribution, and False Target Location Mapping.

3.1. Pulse Compression

Pulse compression is a common signal-processing method in linear frequency modulation pulse compression radar. Its working principle is to extract echo information that is strongly correlated with the reference signal. It can compress received echo signal containing interference into narrow pulses [21] and make the compressed echo appear as multiple target peaks.

Pulse compression is performed on the echo signal with ISRJ interference, and its digital expression is as follows:

$$PC(t) = X_r(t) * H(t) \tag{11}$$

where $X_r\left(t\right) = S_r\left(t\right) + X_{ISRJ}\left(t\right) + n(t)$ is the received echo signal. $S_r\left(t\right) + X_{ISRJ}\left(t\right)$ is the echo of the real target signal mixed with ISRJ interference. $n(t)$ is environmental noise. $H(t)$ is the LFM pulse compression radar matched filter function. $PC(t)$ is the echo pulse compression results.

3.2. Short-Time Fourier Transform

The short-time Fourier Transform (STFT) can be used for the time-frequency analysis of signals, through which more detailed time-frequency characteristics of signals can be obtained [22, 23].

Unlike the Fourier transform, which converts the whole signal from the time domain to frequency domain, the principle of STFT is to divide the whole signal into multiple short-time segments of equal length and use the Discrete Fourier Transform (DFT) to reveal the time-frequency characteristic of each short-time segment.

The principle of the short-time Fourier transform is shown in Fig. 4.

The operation steps for performing the short-time Fourier transform on the echo pulse compression results are as follows:

Step 1: Move a narrow window at equal distances several times in the time domain, and divide the echo pulse compression results into multiple short-time segments of equal length.

Step 2: Use the narrow window time-windowing these short-time segments.

Step 3: Obtain Frequency Energy Density Distribution (FEDD) Information of each short-time segment via discrete Fourier transform.

Set the narrow window as $w(n)$, the sampling points length of the narrow window as l_w, the length of the sampling points where the front and rear windows overlap while moving as $l_{noverlap}$, and $D = \lfloor (PC(n) - l_{noverlap}) / (l_w - l_{noverlap}) \rfloor$ as the number of short-time segments. $l_D = l_w - l_{noverlap}$ is the sampling point length of a short-time segment. $STFT_i(f)$ is the FEDD of the ith short-time segment, $W = nfft/2 - 1$ the frequency length of $STFT_i(f)$, and $nfft$ the number of discrete Fourier transform points. $STFT_i(f)$ can be expressed as:

$$STFT_i(f) = \sum_{n=il_D}^{il_D+l_D-1} w(n)PC(n)e^{-j2\pi fn} \tag{12}$$

3.3. Energy Peak Detection

Energy peak detection is used to detect energy peaks or higher energy parts in a signal. The steps of energy peak detection are as follows:

Step 1: Sum the energy in the frequency domain of each short-time segment after STFT. The summation of the ith short-time segment's energy can be expressed as:

$$P_i = \int_f |STFT_i(f)|^2 \, df \tag{13}$$

Step 2: Set an energy threshold to filter out those short-time segments of lower energy and extract higher energy's short-time segment. Due to different threshold settings that can lead to different filtering results, this paper presents an adaptive threshold algorithm. Set the threshold to the mean of all short-time segment energies summation plus one time their standard deviation to

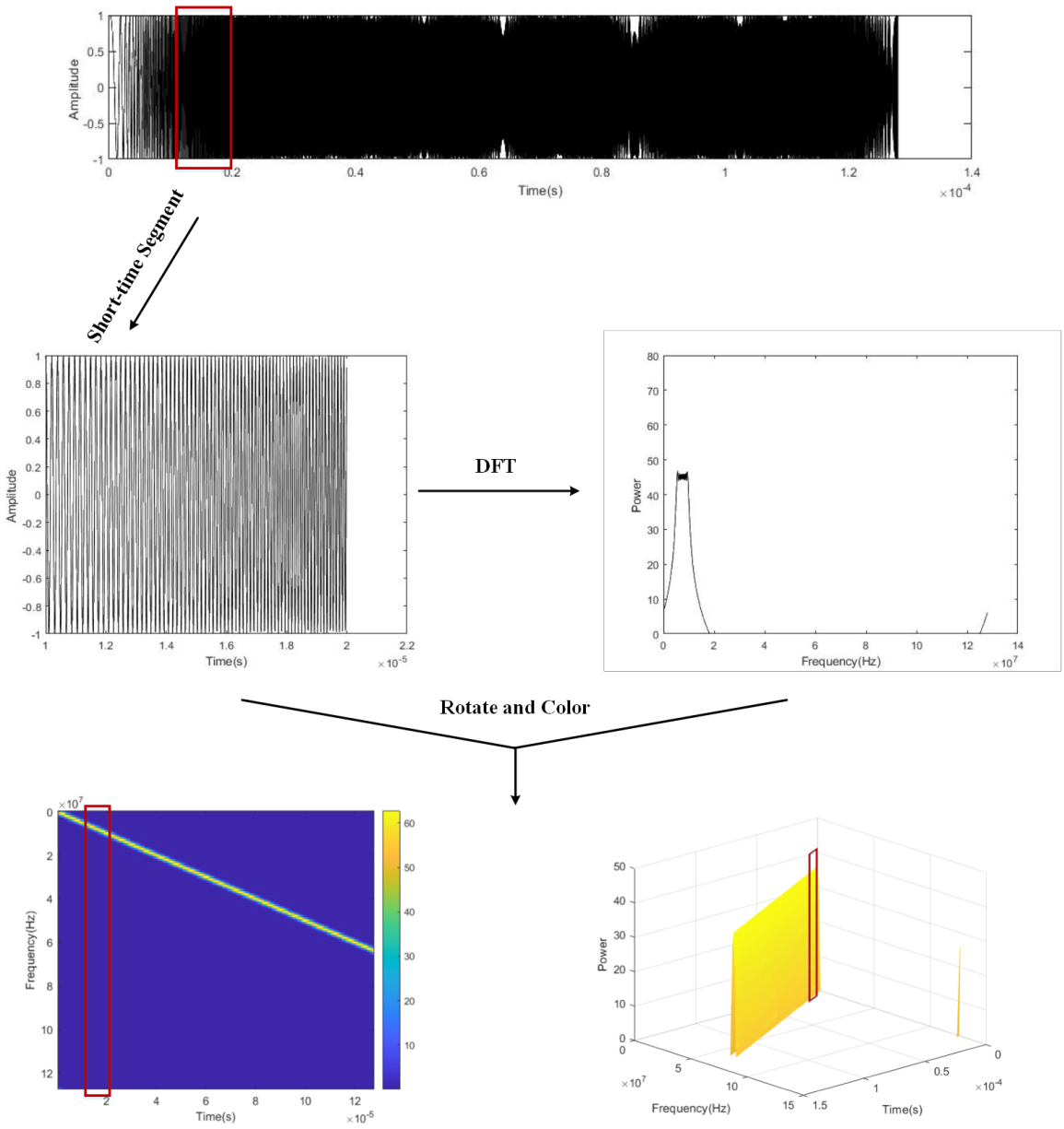

FIGURE 4. The principle of STFT.

extract the high-energy portion that exceeds one time the variability of the average energy sum.

The mathematical expression of the threshold is:

$$P_{threshold} = \bar{P} + \sigma_P \tag{14}$$

where $\bar{P}$ is the mean of these short time segment energies. σ_P is the standard deviation of these short time segment energies summation.

The mathematical expression of $\bar{P}$ is as follows:

$$\bar{P} = \frac{\sum_{i=1}^{D} P_i}{D} \tag{15}$$

where D is the number of short-time segments.

The mathematical expression of σ_P is as follows:

$$\sigma_P = \sqrt{\frac{\sum_{i=1}^{D} \left(P_i - \bar{P}\right)^2}{D}} \tag{16}$$

The principle of Peak Detection is to find the local maximum value in a data sequence, detect whether the value of that point is greater than the value of adjacent two points, and also require that the value of that point exceeds the adaptive threshold. The expression of Peak Detection is:

$$\begin{cases} P_i < P_{i+1} \\ P_{i+2} < P_{i+1} \\ P_{i+1} > P_{threshold} \end{cases} \quad (i = 1, 2, 3, \ldots, D-2) \tag{17}$$

Step 3: Calculate and record the width of each peak. Based on the values of the highest peaks in Step 2, this paper takes the intersection distance between the threshold value and this wave peak as the peak width of this wave peak. The general methods for calculating the peak width of a signal include half maximum width [24] and integration method [25]. Due to the influence of pulse compression results and the large energy summation, this article adopts the method that uses the threshold value to truncate this peak to calculate the peak of width.

Step 4: Construct a Target Time Slice. Retain the time position of the highest point of energy summation for higher energy's short time segments, and use it as the time position for the target time slice. Using the frequency range energy of the time position as the frequency range energy distribution of the target time slice. Set num as the number of higher energy's short time segments extracted by Energy Peak Detection.

Step 5: Sort the constructed target time slices by time order, and record the time position. Set $L = [L_1, L_2, L_3, \ldots, L_n, \ldots, L_{num}]$ as the time position series of target time slices. The intersection points between the peak with the highest peak L_n and the threshold are $L_{n\_\min}$ and $L_{n\_\max}$, then the peak width is $(L_{n\_\max} - L_{n\_\min}) * l_D$, and l_D is the sampling point length of a short-time segment.

Due to the construction of the Target Time Slice based on limiting the low energy target, this method is ineffective for blanket jamming [26].

3.4. Correlation Judgment of Frequency Domain Energy Distribution

The principle of Correlation Judgment of Frequency Domain Energy Distribution is to treat the frequency domain energy distribution of each target time slice as a dependent variable with frequency and reflect the difference of the energy distribution through the linear correlation degree of each dependent variable.

Two methods exist for Correlation Judgment of Frequency Domain Energy Distribution, and they both rely on Pearson Correlation Coefficient (PCC) computations. Set L_e as the time position of the eth target time slice, and $L_{-e} = [L_1, L_2, \ldots, L_{e-1}, L_{e+1}, \ldots, L_{num-1}]$ as the time position of all target time slices except for the eth one. $L = [L_1, L_2, \ldots, L_{e-1}, L_e, L_{e+1}, \ldots, L_{num}]$ is the time position of all targets time slices. Set a target time slice corresponding to a target, and the frequency domain energy distribution correlation of the target time slice corresponds to the correlation between various targets.

The Pearson correlation coefficient is a calculation method, and it measures the strength of the linear correlation between two sequences. If the PCC is close to 1, then the two sequences have a strong correlation. Set $FPED_{L_n}$ as the Frequency Domain Energy Distribution of the nth target time slice. L_n represents the time position of the nth target time slice. The expression of $FPED_{L_n}$ is:

$$FPED_{L_n}(f, P) = |STFT_{L_n}(f)|^2 \tag{18}$$

The mathematical expression of PCC is as follows:

$$r_{[L_x, L_y]} = Cov\left(FPED_{L_x}, FPD_{L_y}\right) / \left(\sigma FPED_{L_x} * \sigma FPED_{L_y}\right) \tag{19}$$

where $r_{[L_x, L_y]}$ is the Pearson Correlation Coefficient for L_x and L_y, and $Cov\left(FPED_{L_x}, FPED_{L_y}\right)$ is the covariance of the frequency domain energy distribution for L_x and L_y. $\left(\sigma FPED_{L_x} * \sigma FPED_{L_y}\right)$ is the standard deviation product of the frequency domain energy distribution for L_x and L_y.

Method 1: Create two Target PCC Datasets, and based on the fact that the ranges of these two datasets do not coincide, identify the target with the lowest correlation.

The first Target PCC Datasets are $r_{[L_e, L_{-e(i)}]}$, which are the PCC datasets of the frequency domain energy distribution between the eth target time slice and other target time slices; $[T_{\min}, T_{\max}]$ is the range of $r_{[L_e, L_{-e}]}$. We name 'The first Target PCC Datasets' 'the Current Target Datasets' in the next part of this paper.

The second Target PCC Datasets are $r_{[L_{-e(i)}, L_{-e(j)}]}$, which are the PCC datasets between the frequency domain energy distributions of other target time slices except for the eth target time slice, where $i \neq j$, and $[F_{\min}, F_{\max}]$ is the range of $r_{[L_{-e(i)}, L_{-e(j)}]}$. We just name 'The second Target PCC Datasets'. The Control Datasets' are in the next part of this paper.

The Current Target Datasets represent the correlation between the eth target and other targets. As shown in Fig. 5(a), the blue box contains PCC data that creates the Current Target Datasets of the 1st target, and the red dashed box contains PCC data that creates the Control Datasets.

$T_{\max} \leq F_{\min}$ means that there is no target that has a smaller correlation with the eth target and other targets. Therefore, it can judge the eth target as the real target and the other targets as false targets.

Method 2: Create num Target PCC Datasets and identify the target with the weakest universal correlation [27] based on the fact that the mean of Target PCC Datasets represents the weak universal correlation of its target with the other targets. As shown in Fig. 5(b), each black dashed box contains PCC data that creates the Target PCC Datasets of each target.

Set $r_{[L_e, L_{-e(i)}]}$ as the Target PCC Datasets of the frequency domain energy distribution between the eth target time slice and other target time slices. $\overline{r_{[L_e, L_{-e}]}}$ is the mean value of the eth Target PCC Datasets. The mathematical expression of $\overline{r_{[L_e, L_{-e}]}}$ is as follows:

$$\overline{r_{[L_e, L_{-e}]}} = \frac{\sum_{i=1}^{num-1} r_{[L_e, L_{-e(i)}]}}{num - 1} \tag{20}$$

The mean value of the eth Target PCC Datasets represents the universal trend of correlation between the eth target and other targets, and a smaller mean value indicates that the eth target

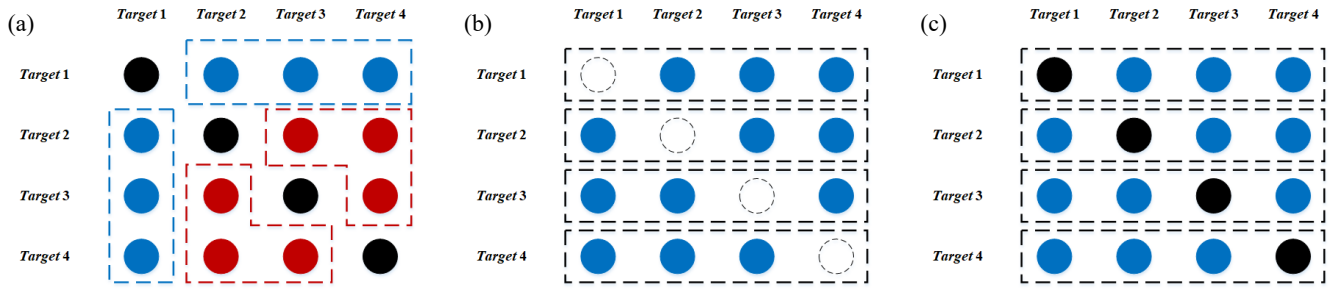

FIGURE 5. The schematic diagram of Target PCC Datasets in the different methods. (a) The Target PCC Datasets in the Method 1. (b) The Target PCC Datasets in the Method 2. (c) The Target PCC Datasets in the Skewness Method.

has a weak universal correlation with the rest of the targets compared to one of the other targets. Therefore, Method 2 judges the eth target as the real target and the other targets as the false targets.

It is important to notice that if there is a low correlation between the frequency domain energy distributions of two targets other than the real target, it will lead to lower robustness of Method 2, and we just name it 'the PCC Singular Values'. The occurrence of the PCC Singular Value can cause the ranges of the Control Datasets and the Current Target Datasets in Method 1 to intersect. Additionally, it results in a very near pair of minimum two means values for the Target PCC Datasets in Method 2.

To solve the problems caused by the PCC Singular Value, the paper proposes an additional method, which is to find the skewness [28] of the Target PCC Datasets. The skewness of the data can indicate whether the number of data is significantly bigger or smaller than the mean value of the data. We just name the additional method 'the Skewness Method'.

Set $r_{[L_e,L(i)]}$ as the Target PCC Datasets of the frequency domain energy distribution between the eth target time slice and all target time slices. $Sco\,(L_e)$ is the Skewness Coefficient of the eth Target PCC Datasets. The mathematical expression of $Sco\,(L_e)$ is as follows:

$$Sco\,(L_e) = (num) \cdot \frac{\sum_{i=1}^{num} \left[X\,(i) - \bar{X}\right]^3}{(num-1)\cdot(num-2)\cdot\sigma_X^3} \tag{21}$$

where $X = r_{[L_e,\underline{L}(i)]}$ represents the Target PCC Datasets of the eth Target. $\bar{X}$ represents the mean of the Target PCC Datasets. σ_X represents the standard deviation of the Target PCC Datasets.

Unlike Method 2, the Target PCC Datasets of each target in the Skewness Method add an autocorrelation PCC of the target. The addition of autocorrelated PCC in the Target PCC Datasets of the Real target is to change the skewness of the datasets. In the Target PCC Datasets of False targets, the addition of autocorrelation PCC is to eliminate the influence of PCC between false targets and the real target on the skewness of the datasets, so as to pay more attention to the influence of the PCC Singular Values. As shown in Fig. 5(c), each black dashed box contains PCC data that creates the Target PCC Datasets of each target.

In Method 2, the PCCs of the Target PCC Datasets of the real target are commonly small, and the PCCs of the Target PCC Datasets of the false target are commonly great. However, in Skewness Method, because the autocorrelation PCC is added to the Target PCC Datasets of the real target, the data number of the Target PCC Datasets that are larger than the mean value increases, and the Skewness Coefficient is greater than 0. The Skewness Coefficient (Sco) of each false target's Target PCC Datasets will have a skewness less than 0 due to the influence of the PCC Singular Values.

The way of creating the Target PCC Datasets proposed in the aforementioned methods is shown in Fig. 5.

The operation flow of the correlation judgment method proposed in this paper is as follows:

Step 1: Calculate the PCC between the Frequency Domain Energy Distributions of each two target time slices. Use the target time slice to represent the target.

Step 2: According to Method 1, create two Target PCC Datasets, and judge the real target by the range of the Current Target Datasets and the Control Target Datasets.

Step 3: According to Method 2, create the Target PCC Datasets of each target, and judge the real target by the minimum mean value of these Target PCC Datasets.

Step 4: According to Skewness Method, add autocorrelation PCC to the Target PCC Datasets in Method 2, and combine the Observation based on the Skewness Coefficient with Method 2 to reduce the influence of the PCC Singular Values on the skewness.

With the correlation judgment being performed on multiple Target PCC Datasets, the limitation of the method is that the number of target time slices by Energy Peak Detection cannot be less than 3. The limitation is referred to as the Target Quantity Limit in this paper.

3.5. False Target Location Mapping

Using the correlation judgment method, the paper can judge the target time slice representing the real and false targets.

Set L_e as the time position of the target time slices representing the real target, and $L_{-e} = [L_1, L_2, \ldots, L_{e-1}, L_{e+1}, \ldots, L_{num-1}]$ is the time position of the target time slices representing the false targets. According to the short-time Fourier transform, $l_D = l_w - l_{noverlap}$ is the length of a short-time segment. According to the energy peak detection, the short-time segment interval corresponding

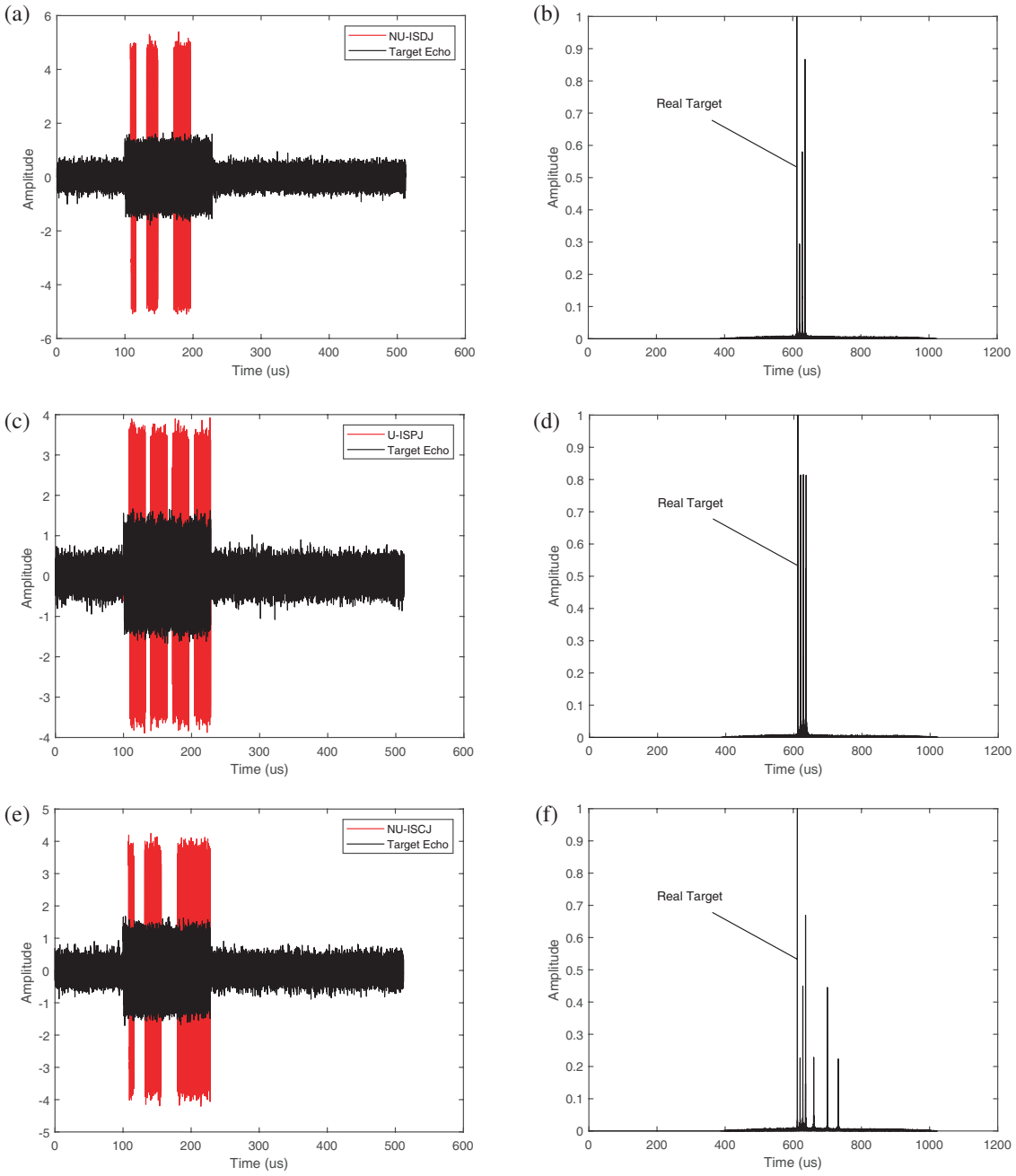

FIGURE 6. The time domain spectrum of echo signals with interference and the result of Pulse Compression.

to the highest energy peak in each short-time segment is $[L_1, L_{num-1}]$. I_n is the mapping interval of the nth false target in the time domain. The expression of I_n is:

$$I_n = [L_{-e\_\min} * l_D - (l_D/2), L_{-e\_\max} * l_D + (l_D/2))] \tag{22}$$

According to the principle of the ISRJ model, the delay of interference and echo signal may lead to the coincidence of the position of the real target and false target in the time domain, as well as the energy superposition in the frequency domain. The situation is known as the Target Coincidence Condition in this paper, and vice versa as the Target Separation Condition.

To meet the situation of the Target Separation Condition, the position relationship between the real target and adjacent false targets must meet the following:

$$\begin{cases} |L_{e\_\min} - L_{e-1\_\max}| < (l_D/2) \\ |L_{e+1\_\min} - L_{e\_\max}| < (l_D/2) \end{cases} \tag{23}$$

4. SIMULATION ANALYSIS

The simulation parameters related to the transmission signal are: the pulse width 128 us, signal bandwidth 64 Mhz, pulse repetition period 512 us, and sampling frequency 128 Mhz. The U-ISPJ interference parameters are: the sampling period width is 32 us; sampling slice width is 8 us; and forwarding time is 3. The environmental parameters are: The signal-to-noise ra-

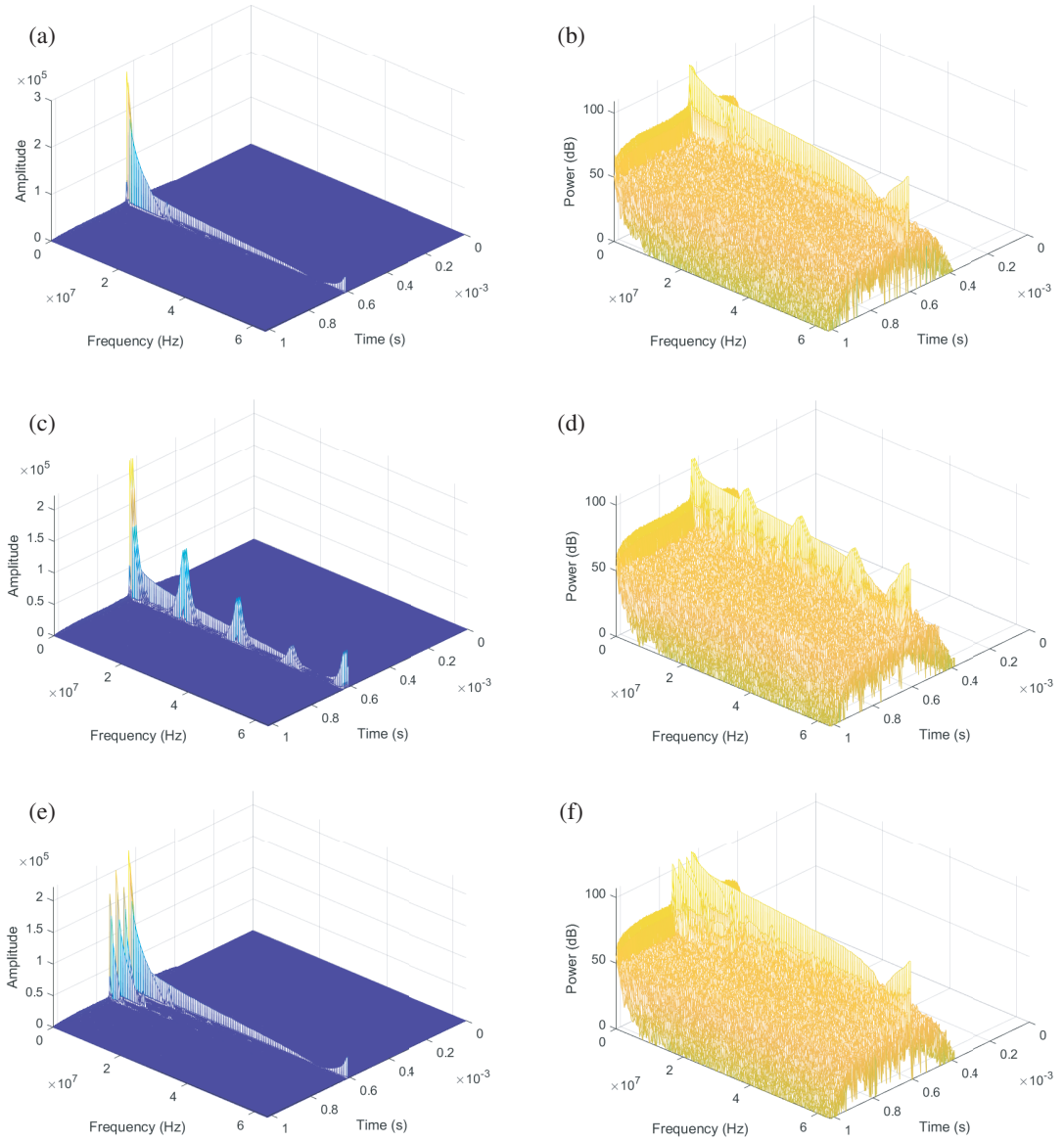

FIGURE 7. The time spectrum diagram of STFT and the energy distribution diagram.

tio (SNR) is 10 dB, and the signal-to-jamming ratio (SJR) is −10 dB.

4.1. The Process Simulation of STFT-EDCJ Method for Echo Signals

The echo signal processing flow of STFT-EDCJ method is shown in Figs. 6–10. Fig. 6 shows the time-domain information of echo signals with interference and the results of Pulse Compression. Fig. 7 shows the energy density spectrum and energy spectrum of the pulse compression results obtained through STFT. Fig. 8 shows a schematic diagram of Peak Detection and the frequency domain energy distribution of high-energy target time slices detected through Peak Detection. Fig. 9 shows the Pearson Correlation Coefficient (PCC) data sets calculated based on the frequency domain energy distribution of each target time slice and the mean value of the PCC Datasets obtained from Method 2. Fig. 10 shows the result of suppressing interference by mapping false targets' time domain intervals. The following three interference models were used in the process simulation in this section: NU-ISDJ, U-ISPJ, and NU-ISCJ.

4.2. The Influence of Interference Model Parameters

According to the principles of the ISRJ model in Section 2, the relevant interference model parameters include the width of the sampling slice, the width of the sampling period, and the maximum value of forwarding times in a sampling period. Under different interference models, the sampling period, sampling slice, and forwarding times affect each other. In addition, other related parameters include input signal-to-noise ratio and input signal-to-interference ratio. In the methods proposed in this article, the simulation values of input signal-to-noise ratio and input signal-to-interference ratio may result in the target time

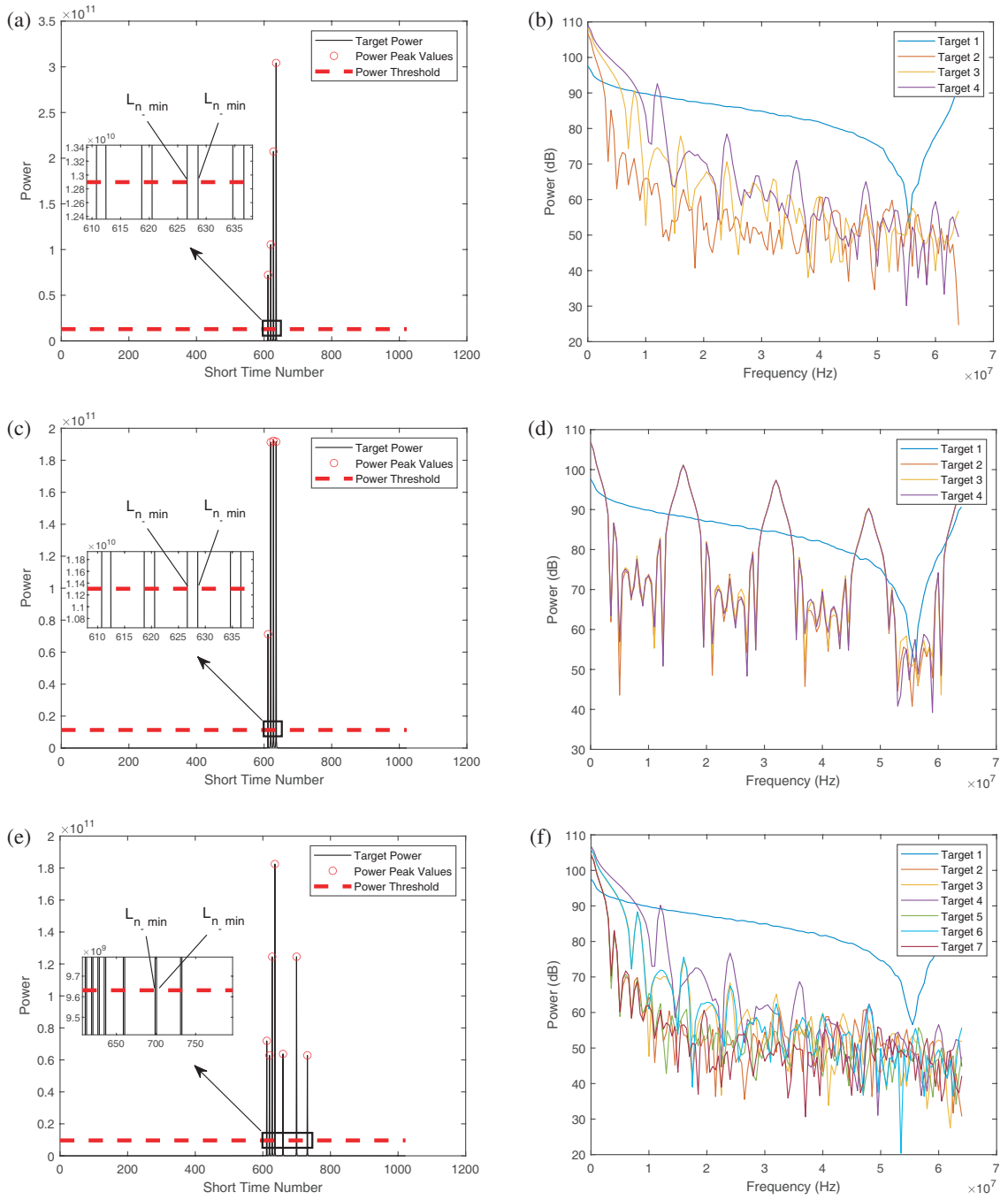

FIGURE 8. The schematic diagram of Peak Detection and the energy distribution diagram of Target Time Slices.

slice representing the real target unable to pass Energy Peak Detection.

To consider the delay of target echo and interference, this paper conducts a simulation analysis of these interference parameters in the Target Separation Condition and Target Coincidence Condition. It should be noted that the Target Coincidence Condition here does not refer to the situation where the jamming and target echo pulse are overlapping in both time and frequency domains, but rather the situation where the narrow pulse of the real target and the narrow pulse of the false target overlap after pulse compression. In this paper, the narrow pulse of the target is referred to as the target time slice.

From Section 2.2, it can be seen that the sampling period width of nonuniform sampling forwarding interference varies with the width of the sampling slice. Therefore, Section 4.2 conducts the following simulation by varying the width of the sampling slice. Through extensive simulation experiments and the principle that noise is generally low-frequency signals, it is known that the input signal-to-noise ratio has little effect on the energy of the target echo and jamming in the frequency domain, and does not affect the energy threshold for peak detection. In this section, the minimum input signal-to-noise ratio was found in the range from -20 dB to 20 dB for different sampling slice widths corresponding to the 1st sampling as shown

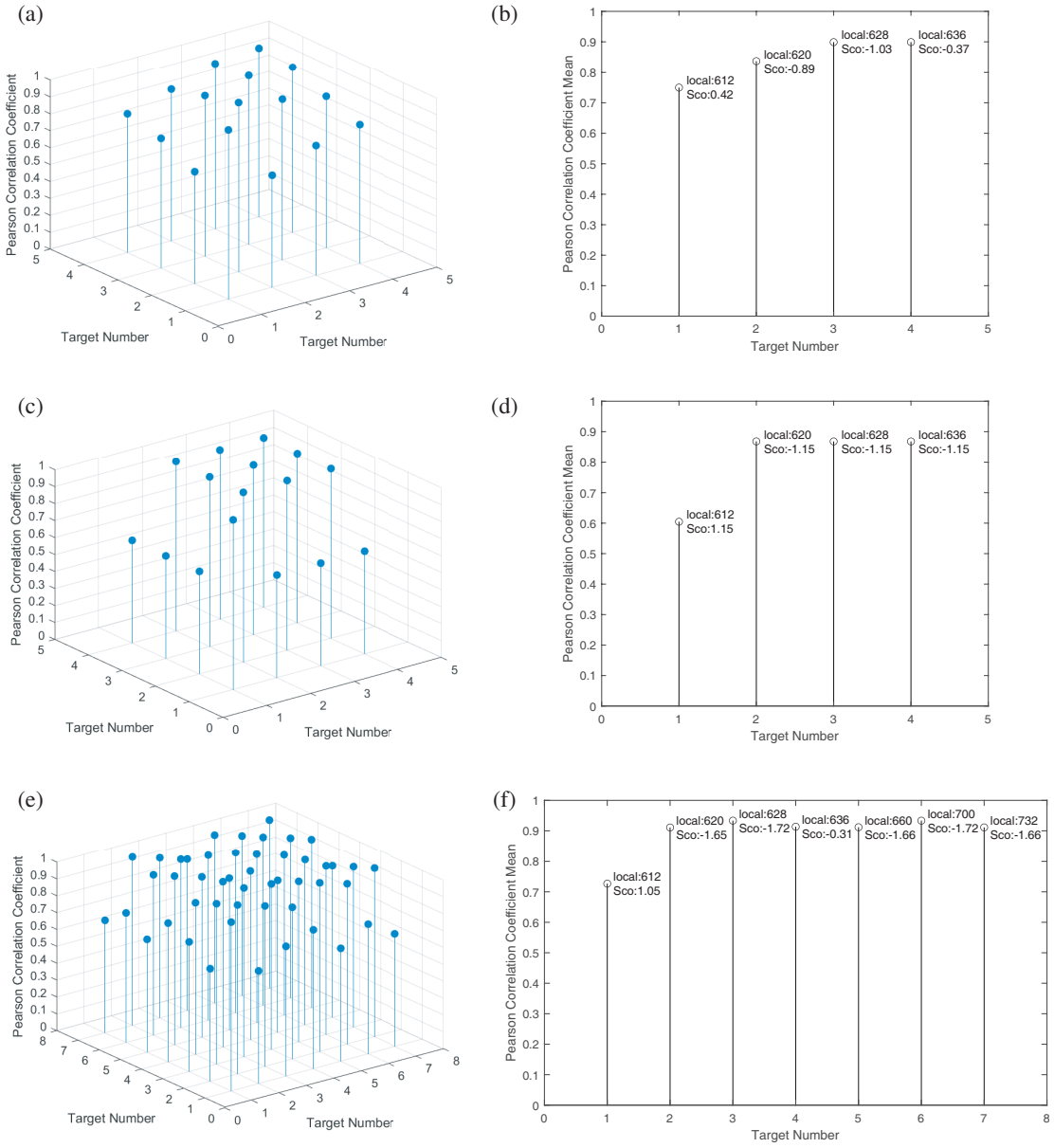

FIGURE 9. The data sets of Person Correlation Coefficient and the PCC mean.

in Figs. 11–15(a). Furthermore, the range of the two datasets of Method 1 for different sampling slice widths corresponding to the 1stsampling is shown in Figs. 11–15(b). The number of Target Time Slices is shown in Figs. 11–15(c). Finally, it is found in the simulation that the number of Target Time Slices has a significant impact on the interference suppression effect under different signal-to-noise ratios. 500 Monte Carlo experiments were conducted to improve the signal-to-noise ratio, and the article uses the Signal-to-Jamming Ratio Improvement Factor (SJRIF) as an evaluation indicator to reflect the interference effect. The results of the SJRIF with changes in signal-to-noise ratio (SNR) are shown in Figs. 11–15(d). SJRIF represents the difference between the input signal-to-jamming ratio and the output signal-to-jamming ratio. It should be noticed that the input signal-to-jamming ratio is a simulated input, which is defined as the ratio of useful signal power to jamming signal power, while the output signal-to-jamming ratio is calculated based on the real target peak and the maximum target peak except for the real target.

4.2.1. Simulation Analysis of ISDJ Interference Parameters

In this paper, the Target Quantity Limit is caused by the correlation judgment method: The number of target time slices by Energy Peak Detection cannot be less than 3. Due to not meeting the Target Quantity Limit, Section 4.2.1 will not conduct simulation analysis on U-ISDJ interference.

The NU-ISDJ interference parameters are set as follows: $\tau_n = K*(n-1)*\tau_1$ represents the width of the sampling slice corresponding to the nth sampling; K represents the growth rate of sampling slice width for each sampling; and τ_1 rep-

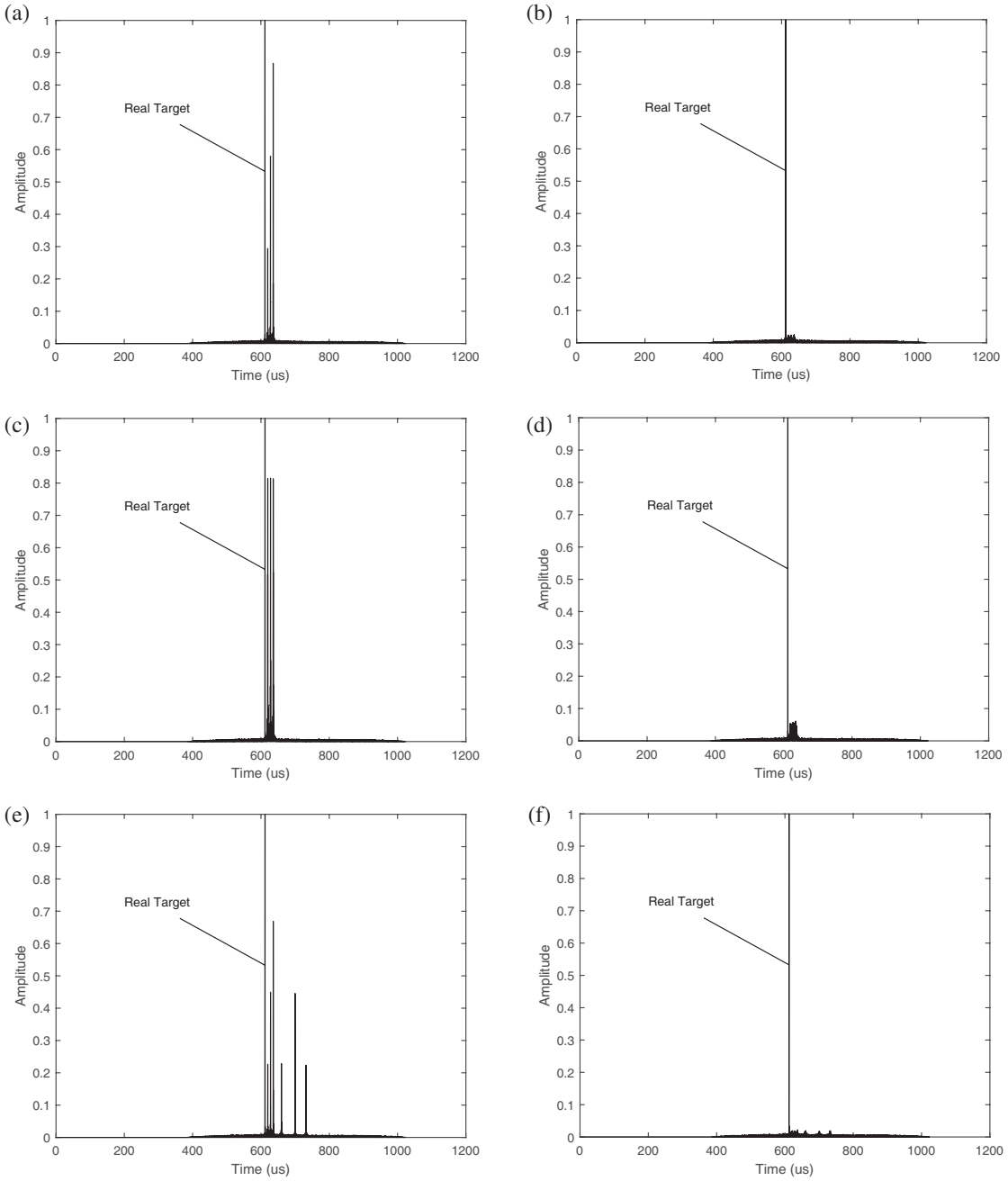

FIGURE 10. The results of before and after Interference Suppression.

resents the width of the sampling slice corresponding to the 1stsampling. $T_s(n) = 2\tau_n$ represents the width of the sampling period corresponding to the nth sampling.

The simulation result for NU-ISDJ in the Target Separation Condition is as follows:

It can be seen from Fig. 11(b2) and Fig. 11(b3) that when the value of K is 2, the value of τ_1 ranges from 2 to 10 us, and when the value of K is 3, the value of τ_1 ranges from 2 to 10 us. There is an intersection between the Current Target Datasets and the Control Target Datasets, and Method 2 is required. The simulation results of Method 2 for NU-ISDJ in the Target Separation Condition are shown in Table 1(a) and Table 1(b).

According to Fig. 11(a1), Fig. 11(a2), and Fig. 11(a3), Energy Peak Detection is not affected by NU-ISDJ interference with the input signal-to-noise ratio higher than -13 dB. According to Fig. 11(b1), Fig. 11(b2), and Fig. 11(b3), Method 1 of the correlation judgment is applicable to NU-ISDJ interference within most parameter ranges. It should be noted that the range of the width of the first sampling slice is set based on the Target Separation Condition and the characteristics of intermittent sampling. For example, as shown in Fig. 11(b1), when the width of the first sampling slice is less than 2 us, it will lead to a situation where the jamming and target echo pulse overlap in both time and frequency domains. When the first sampling

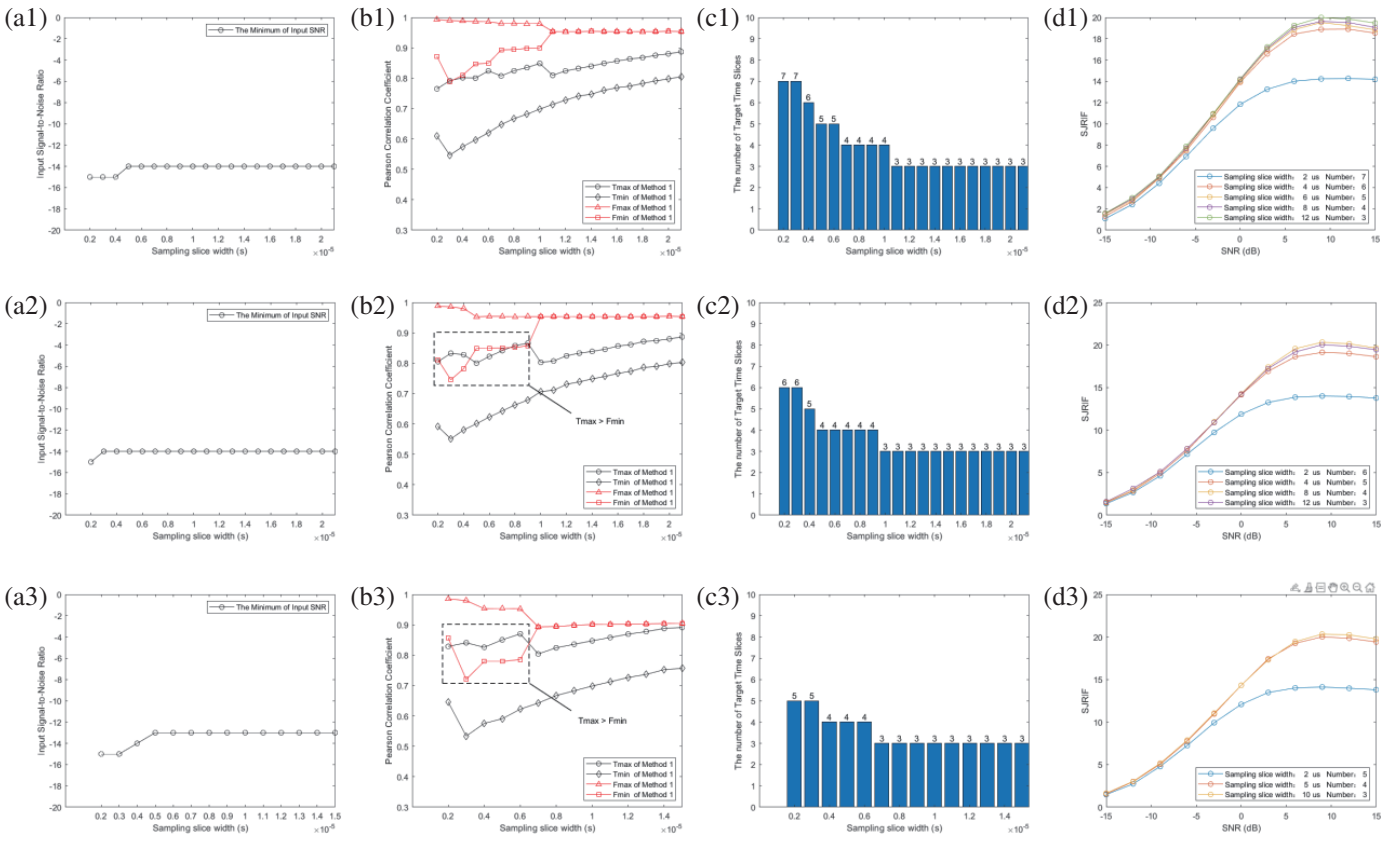

FIGURE 11. The simulation results for NU-ISDJ in the Target Separation Condition. (a) The minimum of input SJR. (b) The simulation results of the Method 1. (c) The number of Target Time Slices. (d) The improvement of SJR under different SNRs. (1) $K = 1$, the value of τ_1 ranges 2–21 us. (2) $K = 2$, the value of τ_1 is 2–21 us. (3) $K = 3$, the value of τ_1 ranges 2–15 us.

slice width is greater than 21 us, interference will lose the characteristic of intermittent sampling. According to Fig. 11(c1), Fig. 11(c2), and Fig. 11(c3), as the sampling slice's width increases, the number of target time slices increases. The growth rate of sampling slice width for each sampling has little impact on the number of Target Time Slices. It can be seen from the Monte Carlo experiments of Fig. 11(d) that the smaller the number of target time slices is, the better the interference suppression effect is. As can be seen from Table 1(a) and Table 1(b), when Method 1 is not satisfied, the difference between the smallest mean value and the second smallest mean value will be too small. Set dm as the difference. $dm < 0.1$ indicates that the robustness of the Method 2 is not strong. The Skewness Method will work in this case. The Skewness Coefficient (Sco) of the smallest mean datasets is greater than 0, while the Sco of the second smallest mean datasets is less than 0. Therefore, when the difference between the two means is small enough, the real target can be judged by the value of the Skewness Coefficient.

4.2.2. Simulation Analysis of ISPJ Interference Parameters

The U-ISPJ interference parameters are set as follows: The sampling period width and sampling slice width are the same for each sampling. τ_1 represents the width of the sampling slice corresponding to the 1st sampling. $T_s(n) = T_s$ represents the width of the sampling period corresponding to the nth sampling. $M = \lfloor T_s/\tau_1 \rfloor - 1$ represents the forwarding times. The simulation result for U-ISPJ in the Target Separation Condition is shown in Fig. 12.

The NU-ISPJ interference parameters are set as follows: $\tau_n = K*(n-1)*\tau_1$ represents the width of the sampling slice corresponding to the nth sampling; K represents the growth rate of sampling slice width for each sampling; and τ_1 represents the width of the sampling slice corresponding to the 1stsampling. $T_s(n) = (M+1)\tau_n$ represents the width of the sampling period corresponding to the nth sampling. $M \geq 2$ represents the forwarding times. The simulation results for NU-ISPJ in the Target Separation Condition are shown in Fig. 13.

According to Fig. 12(a) and Fig. 13(a), Energy Peak Detection is not affected by ISPJ interference with the input signal-to-noise ratio higher than -14 dB. According to Fig. 12(b) and Fig. 13(b), the Current Target Datasets and Control Datasets in Method 1 have a large range gap, which indicates that Method 1 can fully apply ISPJ interference. From Fig. 12(c) and Fig. 13(c), the number of target time slices increases with the increase of the forwarding times. From Fig. 13(c), K has little effect on the number of target time slices. As can be seen from Fig. 12(d) and Fig. 13(d), when input SNR is greater than

TABLE 1. (a) The simulation results of the Method 2 for NU-ISDJ in the Target Separation Condition ($K = 2$). (b) The simulation results of the Method 2 in the Target Separation Condition ($K = 3$).

Parameter	**Value**								
K	**2**								
τ_1 (us)	2	3	4	5	6	7	8	9	10
The smallest mean (Target Location: 545)	0.712	0.725	0.724	0.719	0.744	0.758	0.780	0.785	0.759
The second smallest mean (Target Location: 547)	0.815	0.809	0.818	0.823	0.832	0.833	0.842	0.842	0.838
The difference between the smallest two mean	0.103	0.084	0.094	0.104	0.088	0.075	0.062	0.057	0.079
The Sco of the smallest mean datasets	0.549	0.318	0.413	0.503	0.405	0.319	0.361	0.321	0.430
The Sco of the second smallest mean datasets	−0.669	−0.699	−0.795	−0.843	−0.793	−0.753	−0.690	−0.664	−0.656

(a)

Parameter	**Value**					
K	**3**					
τ_1 (us)	2	3	4	5	6	7
The smallest mean (Target Location: 545)	0.721	0.729	0.729	0.748	0.775	0.739
The second smallest mean (Target Location: 547)	0.763	0.766	0.780	0.785	0.795	0.789
The difference between the two smallest means	0.042	0.037	0.051	0.037	0.020	0.050
The Sco of the smallest mean datasets	0.149	0.027	0.164	0.020	0.004	0.168
The Sco of the second smallest mean datasets	−0.339	−0.422	−0.511	−0.466	−0.343	−0.506

(b)

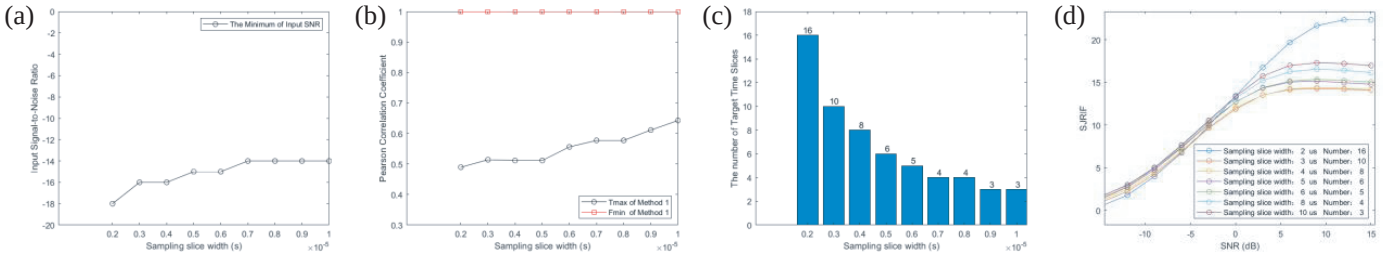

FIGURE 12. The simulation results for U-ISPJ in the Target Separation Condition. (a) The minimum of input SJR. (b) The simulation results of the Method 1. (c) The number of Target Time Slices. (d) The improvement of SJR under different SNRs. The value of τ_1 ranges 2–10 us.

3 dB, the interference suppression effect becomes better with the decrease of the number of target time slices.

4.2.3. Simulation Analysis of ISCJ Interference Parameters

The U-ISCJ interference parameters are set as follows: The sampling period width is the same for each sampling. $T_s(n) = T_s$ represents the width of the sampling period corresponding to the nth sampling. $\tau_n \leq \lfloor T_s / (\lfloor T_P/T_s \rfloor + 1) \rfloor$ represents the width of the sampling slice corresponding to the nth sampling. $M = n$ represents the forwarding times corresponding to the nth sampling. The simulation result of the method proposed in this paper for U-ISCJ in the Target Separation Condition is shown in Fig. 14.

The NU-ISCJ interference parameters are set as follows: $M = n$ represents the forwarding times corresponding to the nth sampling. $T_s(n)$ represents the width of the sampling period corresponding to the nth. τ_n represents the width of the

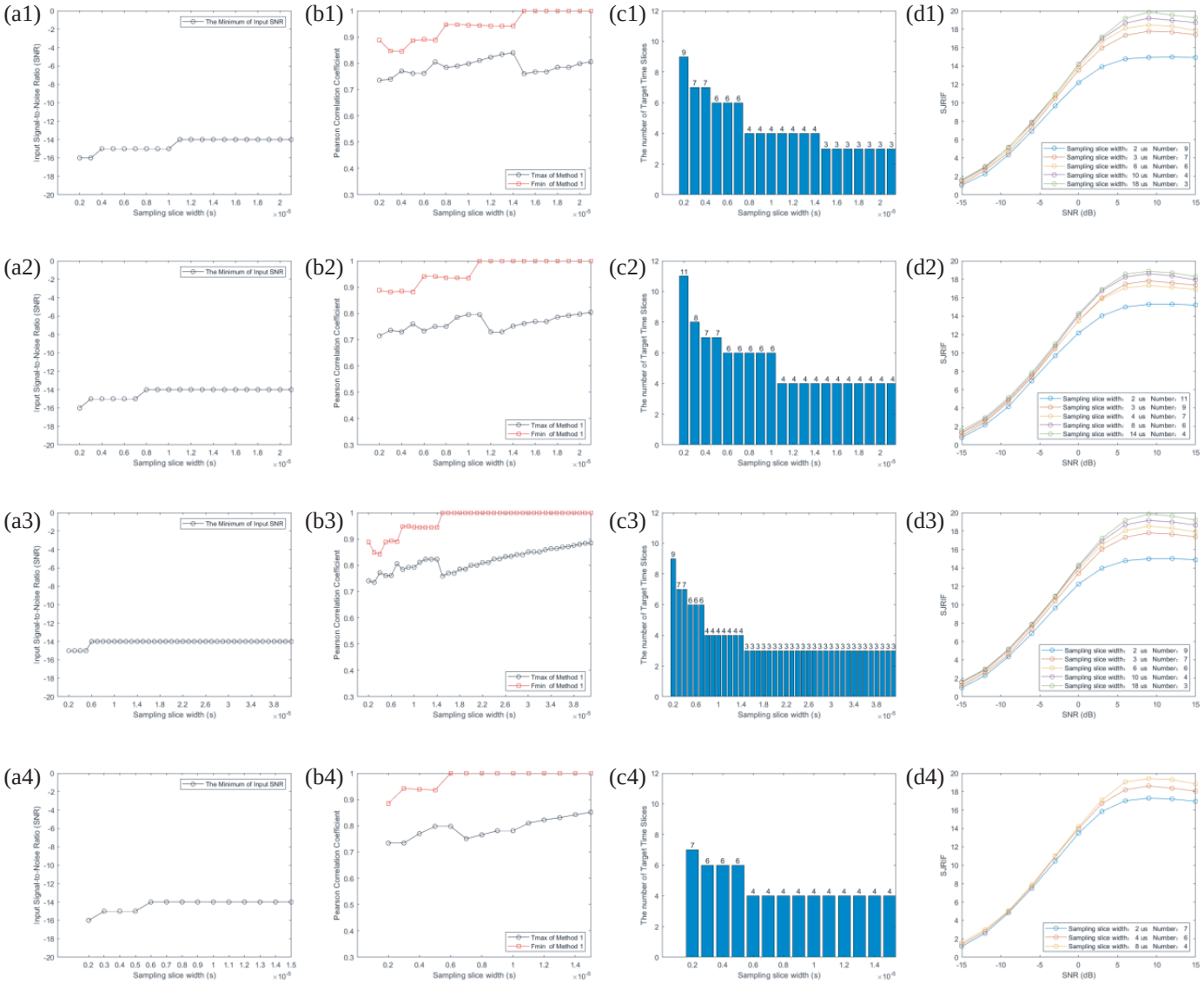

FIGURE 13. The simulation results for NU-ISPJ in the Target Separation Condition. (a) The minimum of input SJR. (b) The simulation results of the Method 1. (c) The number of Target Time Slices. (d) The improvement of SJR under different SNRs. (1) $K = 1$, $M = 2$, the value of τ_1 ranges 2–21 us. (2) $K = 1$, $M = 3$, the value of τ_1 is 2–21 us. (3) $K = 2$, $M = 2$, the value of τ_1 ranges 2–41 us. (4) $K = 2$, $M = 2$, the value of τ_1 ranges 2–41 us.

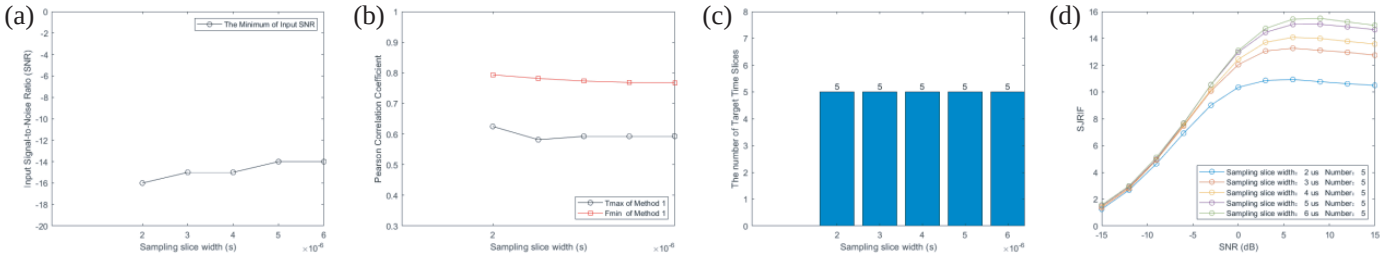

FIGURE 14. The simulation result for U-ISCJ in the Target Separation Condition. (a) The minimum of input SJR. (b) The results of the Method 1. (c) The number of Target Time Slices. (d) The improvement of SJR under different SNRs. The value of τ_1 ranges 2–6 us.

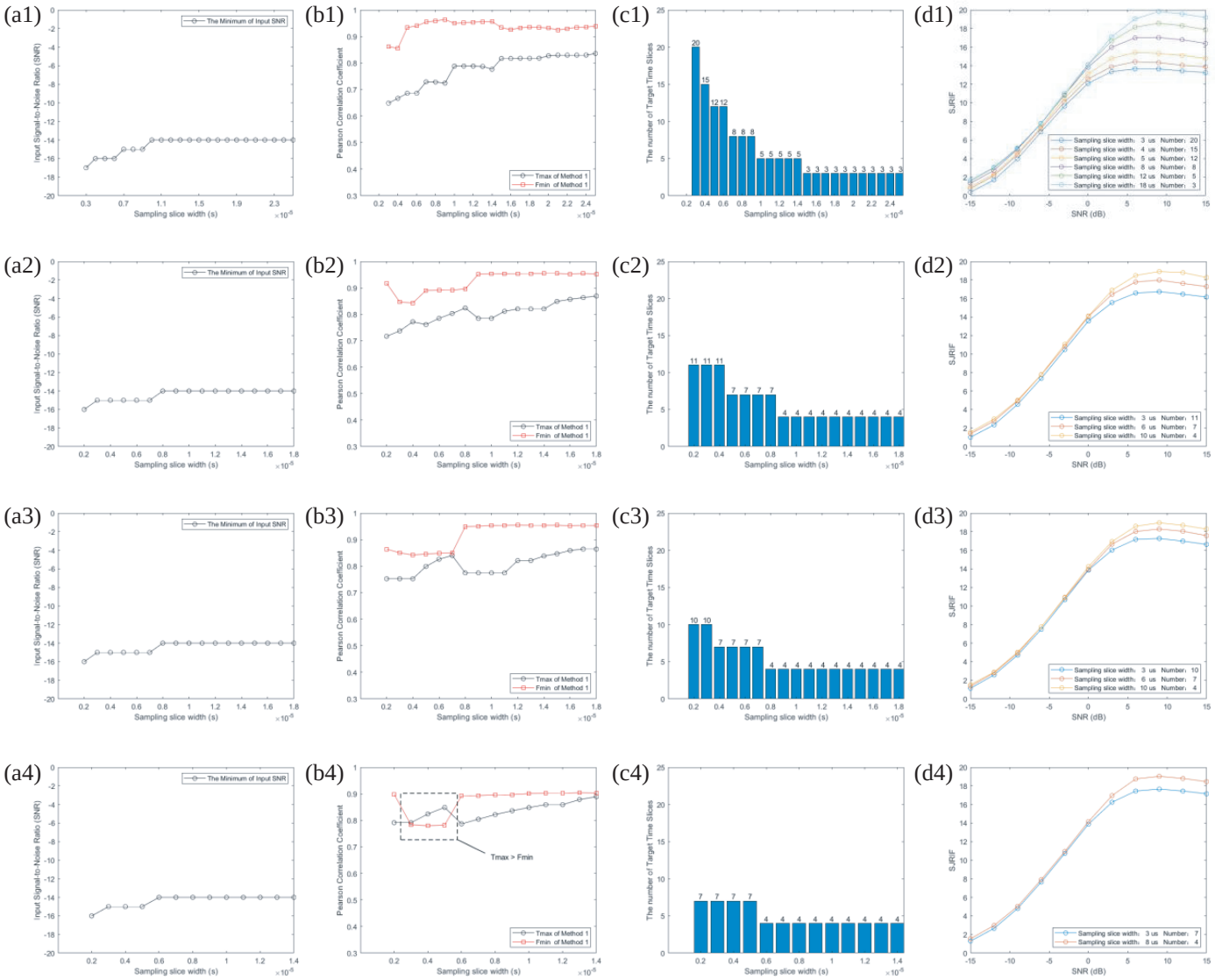

FIGURE 15. The simulation result for NU-ISCJ in the Target Separation Condition. (a) The minimum of input SJR. (b) The results of the Method 1. (c) The number of Target Time Slices. (d) The improvement of SJR under different SNRs. (1) $\tau_n = \tau_1$, the value of τ_1 ranges 3–25 us. (2) $K = 1$, the value of τ_1 ranges 2–18 us. (3) $K = 2$, the value of τ_1 ranges 2–18 us. (4) $K = 3$, the value of τ_1 ranges 2–14 us.

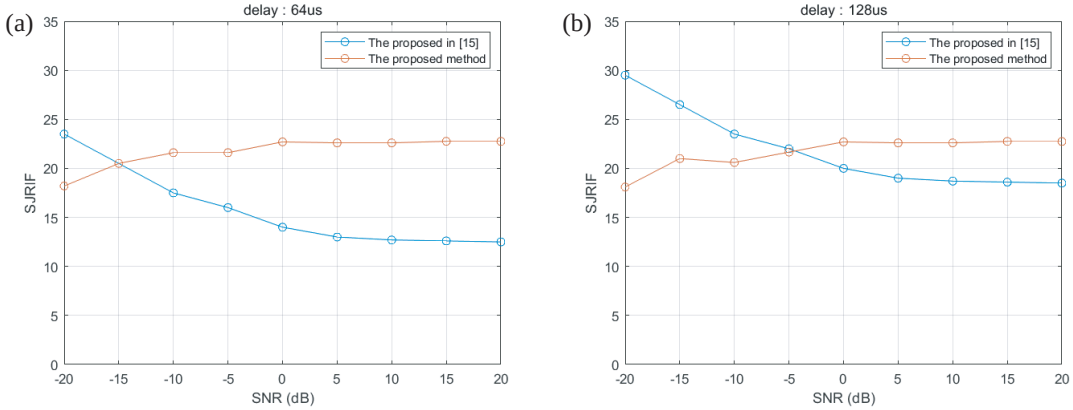

FIGURE 16. The simulation result of the Signal-to-Jamming Ratio Improvement Factor (SJRIF) with changes in signal-to-noise ratio (SNR). (a) The interference delay is 64 us. (b) The interference delay is 128 us.

TABLE 2. The simulation results of the Method 2 for NU-ISCJ in the Target Separation Condition.

Parameter	Value				
K	**3**				
τ_1 (us)	2	3	4	5	6
The smallest mean (Target Location: 545)	0.653	0.657	0.688	0.701	0.704
The second smallest mean	0.861	0.863	0.864	0.867	0.858
The difference between the two smallest means	0.208	0.206	0.176	0.166	0.154
The Sco of the smallest mean datasets	1.021	0.912	0.764	0.636	0.678
The Sco of the second smallest mean datasets	0.053	0.084	0.124	0.122	−0.323

TABLE 3. The simulation results of the Method 2 for U-ISPJ in the Target Coincidence Condition.

Parameter	Value						
K	**2**						
τ_1 (us)	2	3	4	5	6	7	8
The smallest mean	0.814	0.798	0.793	0.760	0.726	0.646	0.645
The second smallest mean	0.925	0.879	0.870	0.799	0.749	0.657	0.655
The difference	0.111	0.081	0.077	0.039	0.023	0.011	0.010
The Sco of the smallest mean datasets	3.55	2.45	2.04	1.49	1.15	0.69	0.71
The Sco of the second smallest mean datasets	−3.57	−2.47	−2.04	−1.5	−1.16	−0.70	−0.71

sampling slice corresponding to the nth sampling. K represents the growth rate of sampling slice width for each sampling. From Section 2, it can be seen that there are two types of sampling slice widths for each sampling of NU-ISCJ. The simulation result of the method proposed in this paper for NU-ISCJ in the Target Separation Condition is shown in Fig. 15.

It can be seen from Fig. 15(b4) that when the value of K is 3, the value of τ_1 ranges from 2 to 6 us. There is an intersection between the Current Target Datasets and Control Target Datasets, and Method 2 is required. The simulation results of Method 2 are shown in Table 2.

According to Fig. 14(a) and Fig. 15(a), Energy Peak Detection is not affected by ISCJ interference with the input signal-to-noise ratio higher than -14 dB. According to Fig. 14(b) and Fig. 15(b), Method 1 of correlation judgment is applicable to U-ISCJ and NU-ISCJ interference within most parameter ranges. As can be seen from Table 2, the difference between the smallest mean value and the second smallest mean value is obvious, so Method 2 can be applied to the case that Method 1 is not satisfied. Set dm as the difference, and $dm > 0.1$. From Fig. 14(b), the smaller the number of target time slices is, the better the interference suppression effect is. From the Monte Carlo experiment results of U-ISCJ, when the number of target time slices is constant, the interference suppression effect becomes better with the increase of the width of the sampling slice. From the Monte Carlo experiment results of NU-ISCJ, the interference suppression effect becomes better with the reduction of the number of target time slices.

4.2.4. Simulation Analysis of ISRJ in the Target Coincidence Condition

From the perspective of correlation judgment methods, this paper regards the problem of position overlapping the real target and false targets as the superposition of target time slice energy in the frequency domain. During simulation, the superposition of the energy distribution in the frequency domain of the target time slice will inevitably lead to an increase in the mean of the Target PCC Datasets representing the real target in Method 2, decreasing the difference between the smallest mean value and the second smallest mean value.

This article will sequentially superimpose the frequency domain energy distribution of the real target onto the frequency domain energy distribution of each group of false targets from the simulation of the Target Separation Condition. Through extensive simulation, it has been found that only U-ISPJ interference maintains a good ability to distinguish real target and false targets in the Target Coincidence Condition. The simulation results of Method 2 for U-ISPJ are shown in Table 3.

From Table 3, the difference between the mean values of U-ISPJ for Method 2 decreases with the decrease in the number of target time slices. Due to the small difference, Method 2 cannot be used for judgment, and the Skewness Method needs to be used. The Skewness Coefficient of the real target's Target PCC Datasets is greater than 0, and the Skewness Coefficient of the Target PCC Datasets for the second minimum mean value is less than 0. It indicates that in the Target Coincidence Condition, the Skewness Method can judge the false targets generated by U-ISPJ interference.

5. COMPARISON EXPERIMENT

Section 5 aims to explore and analyze the effect of interference suppression of the method proposed in this paper in comparison to the method proposed in [15].

Paper [15] segments the echoes throughout the entire pulse cycle and then uses fractional Fourier transform to determine whether this segment of echoes is mixed with interference. The limitation of [15] is that it cannot handle the interference mixed within the target echo pulse. Therefore, under the condition of consistent experimental parameters, we use two scenarios of interference delay of 64 us and 128 us to simulate whether the interference pulse is mixed with the target echo pulse. The simulation experimental parameters settings are shown in Table 4. The simulation results are shown in Fig. 16.

TABLE 4. Simulation experimental parameters.

Parameter	Value
Pulse width	128 us
Bandwidth	32 MHZ
Carrier frequency	35 GHZ
Pulse repetition period	1280 us
ISPJ sampling slice width	8 us
ISPJ sampling period width	40 us
ISPJ forwarding times of each slice	4
ISPJ interference delay	64 us/128 us
SJR (signal-jamming ratio)	-6 dB
SNR (Signal to Noise Ratio)	3 dB
Iteration number	500

From Fig. 16, it can be seen that the interference suppression effect obtained by using the method proposed in this paper and the method proposed in [15] is diverse in different signal-to-noise ratios (SNRs) and whether the target echo pulses are mixed with interference. From Fig. 16(a), when U-ISPJ is mixed in the target echo pulse and the SNR higher than -15 dB, the interference suppression effect of the method proposed in this paper is better than that of the method proposed in [15]. From Fig. 16(b), when there is no mixed U-ISPJ interference in the target echo pulse, and the SNR is higher than -5 dB, the method proposed in this article can achieve a better interference suppression effect.

6. CONCLUSION

This article proposes two methods based on the Correlation Judgment of Frequency Domain Energy Distribution and an additional method which aims to find the skewness to eliminate the influence of the PCC Singular Value and conducts simulation experiments on various Interrupted Sampling Repeater Jamming. We draw the following conclusions from the experimental results:

Conclusion 1: The proposed method has good recognition performance for Interrupted-sampling and periodic repeater jamming (ISPJ), taking into account the overlap between real and false targets caused by interference delay. After ignoring the interference delay, the proposed method can also be applied to Interrupted-sampling and direct repeater jamming (ISDJ) and Interrupted-sampling and cyclic repeater jamming (ISCJ).

Conclusion 2: From the perspective of different sampling modes, this method has better recognition performance for uniform sampling forwarding interference than for nonuniform sampling forwarding interference.

Conclusion 3: In the nonuniform sampling forwarding interference mode, the setting of the sampling slice width and the growth rate of the sampling slice width will affect the selection of these three methods. For example, from the simulation results under NU-ISDJ interference and NU-ISCJ interference modes, it can be seen that in certain specific sampling slice width ranges, Method 1 cannot meet the recognition of interference and requires the adoption of Method 2 and the Skewness Method. Moreover, as the growth rate of sampling slice width increases, the robustness of method one will decrease.

Conclusion 4: This article suppresses interference by eliminating the time domain interval of false targets. The suppression effect of this interference suppression method in various interference modes varies with the number of target time slices generated by the interference, and the number of target time slices is related to the setting of sampling slice width.

The shortcomings of this method include the following aspects:

Shortcoming 1: The interference suppression method in this paper needs to be optimized. At present, the interference suppression method proposed in this paper is only based on the short-time segment mapping interval of STFT as the theoretical basis for further processing of pulse compression results.

Shortcoming 2: The method and simulation proposed in this article are implemented under the premise of precise interference parameters. Further research is needed on the limiting conditions of various interference mode parameters in subsequent experiments.

ACKNOWLEDGEMENT

This work was supported in part by the Hui Yan Xing Dong (62402010206) and Seed Fund of Research and Development

Center for Multi-Sensor Intelligent Detection and Recognition Technology (ZZJ202103-02).

REFERENCES

[1] Wang, X., J. Liu, W. Zhang, O. Fu, Z. Liu, and X. Xie, "Mathematic principles of interrupted-sampling repeater jamming (ISRJ)," *Science in China Series F: Information Sciences*, Vol. 50, No. 1, 113–123, Feb. 2007.

[2] Feng, D., H. Tao, Y. Yang, and Z. Liu, "Jamming de-chirping radar using interrupted-sampling repeater," *Science China Information Sciences*, Vol. 54, No. 10, 2138–2146, Oct. 2011.

[3] Wei, Z., Z. Liu, B. Peng, and R. Shen, "ECCM scheme against interrupted sampling repeater jammer based on parameter-adjusted waveform design," *Sensors*, Vol. 18, No. 4, 1141, Apr. 2018.

[4] Sparrow, M. J. and J. Cikalo, "ECM techniques to counter pulse compression radar," US Patent 7,081,846, Jul. 2006.

[5] Hanbal, S. B. S., "Technique to counter improved active echo cancellation based on ISRJ with frequency shifting," *IEEE Sensors Journal*, Vol. 19, No. 20, 9194–9199, Oct. 2019.

[6] Zhou, K., D. Li, S. Quan, T. Liu, Y. Su, and F. He, "SAR waveform and mismatched filter design for countering interrupted-sampling repeater jamming," *IEEE Transactions on Geoscience and Remote Sensing*, Vol. 60, 1–14, 2021.

[7] Tai, N., Y. Pan, and N. Yuan, "Quasi-coherent noise jamming to LFM radar based on pseudo-random sequence phase-modulation," *Radioengineering*, Vol. 24, No. 4, 1013–1024, Dec. 2015.

[8] Yuan, H., C.-Y. Wang, X. Li, and L. An, "A method against interrupted-sampling repeater jamming based on energy function detection and band-pass filtering," *International Journal of Antennas and Propagation*, Vol. 2017, 1–9, 2017.

[9] Wu, W., J. Zou, J. Chen, S. Xu, and Z. Chen, "False-target recognition against interrupted-sampling repeater jamming based on integration decomposition," *IEEE Transactions on Aerospace and Electronic Systems*, Vol. 57, No. 5, 2979–2991, Oct. 2021.

[10] Lu, L. and M. Gao, "A truncated matched filter method for interrupted sampling repeater jamming suppression based on jamming reconstruction," *Remote Sensing*, Vol. 14, No. 1, 97, 2021.

[11] Xiong, W., G. Zhang, and W. Liu, "Efficient filter design against interrupted sampling repeater jamming for wideband radar," *EURASIP Journal on Advances in Signal Processing*, Vol. 2017, No. 1, 1–12, 2017.

[12] Wang, Z., Y. Wang, J. Li, W. Yu, Z. Yu, and D. Zhang, "A time-frequency filtering method against interrupted sampling repeater jamming based on histogram energy analysis," in *International Conference on Geographic Information and Remote Sensing Technology (GIRST 2022)*, Vol. 12552, 665–675, SPIE, 2023.

[13] Duan, J., L. Zhang, Y. Wu, and Y. Li, "Interrupted-sampling repeater jamming suppression with one-dimensional semi-parametric signal decomposition," *Digital Signal Processing*, Vol. 127, 103546, 2022.

[14] Lv, Q., Y. Quan, M. Sha, W. Feng, and M. Xing, "Deep neural network-based interrupted sampling deceptive jamming countermeasure method," *IEEE Journal of Selected Topics in Applied Earth Observations and Remote Sensing*, Vol. 15, 9073–9085, 2022.

[15] Li, J., J. Zhou, W. Wang, and M. Liu, "A radar waveform design of mcpc method for interrupted sampling repeater jamming suppression via fractional fourier transform," *Progress In Electromagnetics Research C*, Vol. 129, 1–15, 2023.

[16] Rauf, A., H. L. Li, S. Ullah, L. Meng, B. Wang, and S. C. Ge, "Effects of energetic particle precipitation on PMSE echoes observed by EISCAT UHF radar: A case study," *Geomagnetism and Aeronomy*, Vol. 62, No. 4, 495–504, Aug. 2022.

[17] Li, C.-Z., W.-M. Su, H. Gu, C. Ma, and J.-L. Chen, "Improved interrupted sampling repeater jamming based on DRFM," in *2014 IEEE International Conference on Signal Processing, Communications and Computing (ICSPCC)*, 254–257, IEEE, Aug. 2014.

[18] Liu, M., S. Tao, and Q. Chen, "Countermeasure for interrupted-sampling repeater jamming based on fractional Fourier transformation," in *MATEC Web of Conferences*, Vol. 232, 03037, EDP Sciences, 2018.

[19] Liu, D.-Q., C.-G. Sun, and H.-F. Liu, "Intermittent sampling and frequency shift non-uniform and periodic repeating jamming," *Electronic Information Warfare Technology*, Vol. 34, No. 4, 70–75, 2019.

[20] Zhang, H., Y. Zhu, J. Feng, and Q. Fu, "Nonuniform ISRJ suppression based on time shift alignment and morphological processing," *Journal of Physics: Conference Series*, Vol. 2414, No. 1, 012010, 2022.

[21] Zhang, R., Y. Shen, S. Qiu, J. Yu, and W. Sheng, "Polyphase waveform design for ISRJ suppression based on L-BFGS method," *Digital Signal Processing*, Vol. 133, 103840, 2023.

[22] Sejdic, E., I. Djurovic, and J. Jiang, "Time–frequency feature representation using energy concentration: An overview of recent advances," *Digital Signal Processing*, Vol. 19, No. 1, 153–183, Jan. 2009.

[23] Kim, B., S.-H. Kong, and S. Kim, "Low computational enhancement of STFT-based parameter estimation," *IEEE Journal of Selected Topics in Signal Processing*, Vol. 9, No. 8, 1610–1619, Dec. 2015.

[24] Xia, X., L. Liu, H. Guan, and G. Fang, "Balanced pulse generator for ultra-wideband radar application," *Electronics Letters*, Vol. 49, No. 4, 293–295, Feb. 2013.

[25] Xu, X., G. Liao, Z. Yang, and C. Wang, "Moving-in-pulse duration model-based target integration method for HSV-borne high-resolution radar," *Digital Signal Processing*, Vol. 68, 31–43, Sep. 2017.

[26] Wu, Q., F. Zhao, X. Ai, X. Liu, and S. Xiao, "Two-dimensional blanket jamming against ISAR using nonperiodic ISRJ," *IEEE Sensors Journal*, Vol. 19, No. 11, 4031–4038, Jun. 2019.

[27] Bereczuk, A., B. Dietz, J. Che, J. Kuipers, J.-D. Urbina, and K. Richter, "Universal S-matrix correlations for complex scattering of wave packets in noninteracting many-body systems: Theory, simulation, and experiment," *Physical Review E*, Vol. 103, No. 5, 052209, May 2021.

[28] Ozansoy, C., "Performance analysis of skewness methods for asymmetry detection in high impedance faults," *IEEE Transactions on Power Systems*, Vol. 35, No. 6, 4952–4955, Nov. 2020.